A Bubbling Fluidization Model Using Kinetic Theory of Granular Flow

Detailed knowledge of solids circulation, bubble motion, and frequencies of porosity oscillations is needed for a better understanding of tube erosion in fluidized bed combustors. A predictive two-phase flow model was derived starting with the Boltzmann equation for velocity distribution of particles. The model is a generalization of the Navier-Stokes equations of the type proposed by R. Jackson, except that the solids viscosities and stresses are computed by simultaneously solving a fluctuating energy equation for the particulate phase. The model predictions agree with time-averaged and instantaneous porosities measured in two-dimensional fluidized beds. Observed flow patterns and bubbles were also predicted.

Jianmin Ding
Dimitri Gidaspow
Department of Chemical Engineering
Illinois Institute of Technology
Chicago, IL 60616

Introduction

Quantitative undertanding of the hydrodynamics of fluidization is needed for the design and scale-up of efficient new reactors in the petroleum, chemical and electric power industries (Avidan et al., 1989; Squires et al., 1985). For example, although bubbling fluidized bed combustors have reached a commercial status, an understanding of solids motion and its effect on erosion of the heat exchanger tubes immersed in fluidized beds remains inadequate. Hydrodynamic models have been developed (Bouillard et al., 1989a, b) that have the potential of predicting erosion patterns in fluidized beds. These two fluid models are a generalization of the celebrated Navier-Stokes equations used in single-phase fluid mechanics. They were originally developed by Jackson (1963), Soo (1967), Garg and Pritchett (1975), and others. Gidaspow (1986) has given a complete review and has shown that these models, with zero gas and solids viscosities, were able to predict a great deal of the behavior of bubbling beds because the dominant mechanism of energy dissipation is the drag between the particles and the fluid. The formation, the growth, and the bursting of bubbles were predicted (Gidaspow et al., 1983 a,b) in a qualitative agreement with experiments. Computed wall to bed heat transfer coefficients (Syamlal and Gidaspow, 1985) and velocity profiles of jets (Ettehadieh et al., 1984) agreed with measurements. Time-averaged porosity distributions (Gidaspow et al., 1983b; Bouillard et al., 1989b) agreed with measurements done using gamma ray densitometers without the use of adjustable parameters and without prescribing the porosity at any boundaries in the computation. However, analogous to classical fluid dynamics, inviscid models do not predict the forces acting on the tubes immersed in fluidized beds. Therefore to overcome this deficiency a solids viscosity was added to the model, similar to the treatment of Jackson (1985), to compute erosion rates around the tubes. Unfortunately this solids viscosity and also the solids stress were not known and had to be estimated based on very limited data.

The objective of this paper is to give a model that is capable of predicting this solids viscosity and the solids stress based on first principles. The starting point is the Boltzmann integral-differential equation for velocity distribution of particles. Such an approach without an interstitial fluid was pioneered by Savage (1983, 1988), Jenkins and Savage (1983), and others (Shahinpoor and Ahmadi, 1983; Lun et al., 1984; Johnson and Jackson, 1987). It is based on the kinetic theory of dense gases, as presented by Chapman and Cowling (1970, Ch. 16). In this theory the usual thermal temperature is replaced by a granular flow temperature for which a differential equation is derived using the methods of kinetic theory. Thus the solids viscosity and the solids stress are a function of this granular temperature, which varies with time and position in a fluidized bed.

This new kinetic theory of two-phase flow was incorporated into the IIT fluidization computer code (Gidaspow, 1986) to eliminate the need for using guessed solids viscosities and stresses. The computed results agreed well with experimentally measured time-averaged porosities in a two-dimensional bed and reasonably well with experimentally determined porosity oscillations, after the kinetic theory of solids of Lun et al. (1984) and Jenkins and Savage (1983) was slightly modified and extented to two-phase flow.

Transport Equations for the Solids Phase

Let us define a velocity distribution function $f(\mathbf{r}, \mathbf{c}, t)$ of a large collection of granular particles that satisfies the Boltzmann integral-differential equation,

$$\frac{\partial f}{\partial t} + c_i \frac{\partial f}{\partial x_i} + \frac{\partial}{\partial c_i}(F_i f) = \left(\frac{\partial f}{\partial t}\right)_c \tag{1}$$

where the function f is defined such that $fd\mathbf{c}$ is the differential number of particles per unit volume with velocities within the range $\mathbf{c}$ and $\mathbf{c} + d\mathbf{c}$, F is the external force per unit mass acting on each particle, and $(\partial f/\partial t)_c$ is the rate of change of the distribution function due to the particle collisions.

Taking the ensemble average of the single-particle quantity ψ over Eq. 1, we obtain the transport equation for mean quantity ψ in Cartesian tensor notation (Chapman and Cowling, 1970, Ch. 3) as

$$\frac{\partial}{\partial t}(n\langle\psi\rangle) + \frac{\partial}{\partial x_i}(n\langle c_i\psi\rangle) - n\left[\left\langle\frac{\partial\psi}{\partial t}\right\rangle + \left\langle c_i\frac{\partial\psi}{\partial x_i}\right\rangle + \left\langle F_i\frac{\partial\psi}{\partial c_i}\right\rangle\right] = \phi_c(\psi) \tag{2}$$

in which n is the particle number density,

$$n = \int f d\mathbf{c} \tag{3}$$

and $\langle\psi\rangle$ is the averaged quantity defined as

$$\langle\psi\rangle = \frac{1}{n}\psi f d\mathbf{c} \tag{4}$$

To evaluate $\phi_c(\psi)$, the collisional rate of change of the mean of ψ, we must assume that only binary collisions between hard, smooth, but inelastic particles are dominant. Considering the collision between particles labeled 1 and 2, the probable number of collisions per unit time such that the velocities of particle 1 and particle 2 are in the range of $d\mathbf{c}_1$ and $d\mathbf{c}_2$, respectively, and the center of particle 1 is in the volume $d\mathbf{r}$ is (Chapman and Cowling, 1970, Ch. 16; Jenkins and Savage, 1983)

$$f^{(2)}(\mathbf{c}_1, \mathbf{r}; \mathbf{c}_2, \mathbf{r} + d_p\mathbf{k}; t)\, d_p^2(\mathbf{c}_{12}\cdot\mathbf{k})\, d\mathbf{k}d\mathbf{c}_1 d\mathbf{c}_2 d\mathbf{r} \tag{5}$$

where $f^{(2)}$ is the pair-distribution function. It is defined such that $f^{(2)}d\mathbf{r}_1 d\mathbf{r}_2 d\mathbf{c}_1 d\mathbf{c}_2$ is the probability of finding a pair of particles in the volume element $d\mathbf{r}_1 d\mathbf{r}_2$ centered on the points $\mathbf{r}_1$, $\mathbf{r}_2$ and have a velocity within the range $\mathbf{c}_1$ to $\mathbf{c}_1 + d\mathbf{c}_1$, and $\mathbf{c}_2$ to $\mathbf{c}_2 + d\mathbf{c}_2$. $\mathbf{c}_{12}$ is the relative velocity of particle 1 and particle 2, $\mathbf{k}$ is the unit vector along the line from the center of particle 1 to the center of particle 2 at collision, and $\mathbf{r}_2 - \mathbf{r}_1 = d_p\mathbf{k}$. For a collision it is necessary that the center of the second particle lie in a collision cylinder of volume $d_p^2(\mathbf{c}_{12}\cdot\mathbf{k})d\mathbf{k}$ per unit time. Due to the collision, the property ψ_1 of particle 1 changes to ψ_1'. The collisional rate of change for ψ_1 per unit volume is (Jenkins and Savage, 1983; Lun et al., 1984)

$$\phi_c = \int_{\mathbf{c}_{12}\cdot\mathbf{k}>0}(\psi_1' - \psi_1)(\mathbf{c}_{12}\cdot\mathbf{k})\, d_p^2 f^{(2)}(\mathbf{r}, \mathbf{c}_1; \mathbf{r} + d_p\mathbf{k}, \mathbf{c}_2; t)\, d\mathbf{k}d\mathbf{c}_1 d\mathbf{c}_2 \tag{6}$$

Since the collision is symmetric, we can directly write the collisional rate of change ψ_2 by interchanging the labels 1 and 2 and replacing $\mathbf{k}$ by $-\mathbf{k}$

$$\phi_c = \int_{\mathbf{c}_{12}\cdot\mathbf{k}>0}(\psi_2' - \psi_2)(\mathbf{c}_{12}\cdot\mathbf{k})\, d_p^2 f^{(2)}(\mathbf{r} - d_p\mathbf{k}, \mathbf{c}_1; \mathbf{r}, \mathbf{c}_2; t)\, d\mathbf{k}d\mathbf{c}_1 d\mathbf{c}_2 \tag{7}$$

Expanding $f^{(2)}(\mathbf{r}, \mathbf{c}_1; \mathbf{r} + dp\mathbf{k}, \mathbf{c}_2; t)$ in a Taylor series, upon discarding terms involving spatial derivatives higher than the first,

$$f^{(2)}(\mathbf{r}, \mathbf{c}_1; \mathbf{r} + d_p\mathbf{k}, \mathbf{c}_2; t) = f^{(2)}(\mathbf{r} - d_p\mathbf{k}, \mathbf{c}_1; \mathbf{r}, \mathbf{c}_2; t) + d_p\mathbf{k}\cdot\nabla f^{(2)}(\mathbf{r} - d_p\mathbf{k}, \mathbf{c}_1; \mathbf{r}, \mathbf{c}_2; t)$$

and combining Eqs. 6 and 7, we obtained

$$\phi_c = \nabla\cdot\Theta + \chi \tag{8}$$

where

$$\Theta = \frac{d_p}{2}\int_{\mathbf{c}_{12}\cdot\mathbf{k}>0}(\psi_1' - \psi_1)(\mathbf{c}_{12}\cdot\mathbf{k})\mathbf{k}\, d_p^2 f^{(2)}(\mathbf{r}_1, \mathbf{c}_1; \mathbf{r}_2, \mathbf{c}_2; t)\, d\mathbf{k}d\mathbf{c}_1 d\mathbf{c}_2 \tag{8a}$$

$$\chi = \tfrac{1}{2}\int_{\mathbf{c}_{12}\cdot\mathbf{k}>0}(\psi_2' + \psi_1' - \psi_2 - \psi_1)(\mathbf{c}_{12}\cdot\mathbf{k})\, d_p^2 f^{(2)}(\mathbf{r}_1, \mathbf{c}_1; \mathbf{r}_2, \mathbf{c}_2; t)\, d\mathbf{k}d\mathbf{c}_1 d\mathbf{c}_2 \tag{8b}$$

By taking ψ to be m and using the relation $\epsilon_s\rho_p = nm$, we obtain the standard continuity equation for solids flow,

$$\frac{\partial}{\partial t}(\epsilon_s\rho_p) + \frac{\partial}{\partial x_i}(\epsilon_s\rho_p v_i) = 0 \tag{9}$$

where the mean velocity v_i is defined as given by Eq. 4,

$$v_i = \langle c_i\rangle = \frac{1}{n}\int c_i f d\mathbf{c}$$

Before deriving a momentum equation, we must deal with the external force F_i. In general, F_i includes the gravity, the aerodynamic drag, the buoyancy, the added mass force, the Basset force, the Magnus effect, and the Saffman life force. For gas-solids flow, the last four effects are assumed to be negligible. Then we have

$$F_i = g_i + \frac{D}{m}(c_{gi} - c_i) - \frac{1}{\rho_p}\frac{\partial p_g}{\partial x_i} \tag{10}$$

where D is the drag force coefficient. For model A (Bouillard et al., 1989a) the buoyancy effect appears through the pressure gradient in Eq. 10. For model B it would be deleted. Taking $\psi = mc_i$ and using Eqs. 2 and 10, the velocity-dependent term in the transport equation becomes

$$n\left\langle F_j\frac{\partial}{\partial c_j}(mc_i)\right\rangle = \epsilon_s\rho_p g_i + \epsilon_s\rho_p\frac{D}{m}(u_i - v_i) - \epsilon_s\frac{\partial p_g}{\partial x_i}$$

Then grouping the collision-dependent stresses, we obtain the momentum equation

$$\frac{\partial}{\partial t}(\epsilon_s \rho_p v_i) + \frac{\partial}{\partial x_j}(\epsilon_s \rho_p v_i v_j) = -\epsilon_s \frac{\partial p_g}{\partial x_i} + \epsilon_s \rho_p g_i + \beta(u_i - v_i) + \frac{\partial}{\partial x_j}(\tau_{ij}^k + \tau_{ij}^c) \quad (11)$$

where

$$\beta = \epsilon_s \rho_p \frac{D}{m} \quad (11a)$$

$$\tau_{ij}^k = -\epsilon_s \rho_p \langle C_i C_j \rangle \quad (11b)$$

$$\tau_{ij}^c = \Theta_i(mc_j) \quad (11c)$$

$$C_i = c_i - v_i \quad (11d)$$

From Eq. 11 we see that the total stress tensor τ_{ij} is the sum of a kinetic part τ_{ij}^k and a collisional part τ_{ij}^c. Otherwise, Eq. 11 is again the standard two-phase flow momentum balance.

Similarly, by taking $\psi = 1/2\ (mC^2)$ and using the momentum equation, we obtain the equation for the fluctuating energy,

$$\frac{3}{2}\left[\frac{\partial}{\partial t}(\epsilon_s \rho_p T) + \frac{\partial}{\partial x_j}(\epsilon_s \rho_p v_j T)\right] = \tau_{ij}\frac{\partial v_i}{\partial x_j} - \frac{\partial q_j}{\partial x_j} - \gamma + \beta\langle C_{gi}C_i - C_i C_i\rangle \quad (12)$$

where

$$\tfrac{3}{2}T = \tfrac{1}{2}\langle C^2 \rangle \quad (12a)$$

The collisional energy dissipation γ is

$$\gamma = -\chi(\tfrac{1}{2}mC^2) \quad (12b)$$

$$q_j = q_j^k + q_j^c \quad (12c)$$

and

$$q_j^k = \tfrac{1}{2}\epsilon_s \rho_p \langle C_i C^2 \rangle \quad (12d)$$

$$q_j^c = -\Theta_j(\tfrac{1}{2}mC^2) \quad (12e)$$

On the righthand side of Eq. 12, the first term represents the energy production due to the deformation work, the second term is the energy transfer, the third term is the energy dissipation due to inelastic collisions, and the last term is the net rate of transfer of fluctuation energy between the two phases. This equation differs from Eq. 2.15 of Lun et al. (1984) by the presence of this last term.

In Eq. 12 we assumed that the correlation between the gas phase fluctuation velocity and the solid phase fluctuation velocity C_i is negligible. Such an assumption is valid when the particle response time, $\tau_p = m/D$, is much larger than the time scale characteristic of the mean fluid motion (Pourahmadi and Humphrey, 1983). This assumption is valid when the particles are heavy and large. Another reason to neglect $\langle C_{gi}C_i\rangle$ is the difficulty of estimating the fluctuating interaction of the two phases. Further consideration of the transfer of fluctuation energy between the two phases may require a turbulent model for the gas phase in the presence of the solid phase.

Constitutive Equations

To close the transport equations presented in the preceding section, we need to find the single-particle distribution function $f(\mathbf{r}, \mathbf{c}, t)$ and the pair-distribution function $f^{(2)}(\mathbf{r}_1, \mathbf{c}_1; \mathbf{r}_2, \mathbf{c}_2; \mathbf{t})$. Here, we take the Maxwellian velocity distribution function as the single-particle distribution (Savage and Jeffrey, 1981; Jenkins and Savage, 1983),

$$f(\mathbf{r}, \mathbf{c}, t) = \frac{n}{(2\pi T)^{3/2}} \exp\left[-\frac{(\mathbf{c} - \mathbf{v})^2}{2T}\right] \quad (13)$$

We then obtain the kinetic parts of solid stress τ_{ij}^k and the energy flux q_j^k by Eqs. 11b and 12d as (see Appendix, Eqs. A1–A6)

$$\tau_{ij}^k = -\epsilon_s \rho_p T \delta_{ij} \quad (14)$$

$$q_j^k = 0 \quad (15)$$

The Enskog assumption for the pair-distribution function is used next (Chapman and Cowling, 1970; Lun et al, 1984). That is

$$f^{(2)}(\mathbf{r}_1, \mathbf{c}_1; \mathbf{r}_2, \mathbf{c}_2; t) = g_0(\epsilon_s) f_1(\mathbf{r} - \tfrac{1}{2}d_p\mathbf{k}, \mathbf{c}_1; t) f_2(\mathbf{r} + \tfrac{1}{2}d_p\mathbf{k}, \mathbf{c}_2; t) \quad (16)$$

where g_0 is the equilibrium radial distribution function (Savage and Jeffrey, 1981). Expanding f_1 and f_2 in a Taylor series at the point $\mathbf{r}$, *we have*

$$f^{(2)} = g_0(\epsilon_s)\left[f_1(\mathbf{r}, \mathbf{c}_1, \mathbf{t}) f_2(\mathbf{r}, \mathbf{c}_2, \mathbf{t}) + \frac{1}{2}d_p f_1(\mathbf{r}, \mathbf{c}_1, \mathbf{t}) f_2(\mathbf{r}, \mathbf{c}_2, \mathbf{t})\, \mathbf{k} \cdot \nabla\left(\ln\frac{f_2}{f_1}\right)\right] \quad (17)$$

Using Eq. 17 in Eq. 8 with the velocity relations in a collision (Lun et al., 1984)

$$\mathbf{c}_1' = \mathbf{c}_1 - \tfrac{1}{2}(1 + e)(\mathbf{c}_{12} \cdot \mathbf{k})\mathbf{k} \quad (18a)$$

$$\mathbf{c}_2' = \mathbf{c}_2 + \tfrac{1}{2}(1 + e)(\mathbf{c}_{12} \cdot \mathbf{k})\mathbf{k} \quad (18b)$$

where e is the coefficient of restitution, the integrals yield (see Appendix)

$$\tau_{ij}^c = -2\epsilon_s^2 \rho_p g_0(1 + e) T\delta_{ij} + \frac{4\epsilon_s^2 \rho_p d_p g_0(1 + e)}{3\pi^{1/2}} T^{1/2}\left(\frac{6}{5}S_{ij} + \frac{\partial v_k}{\partial x_k}\delta_{ij}\right) \quad (19)$$

$$q_j^c = -\kappa \frac{\partial T}{\partial x_j} \quad (20)$$

$$\gamma = 3(1-e^2)\epsilon_s^2 \rho_p g_0 T\left[\frac{4}{d_p}\left(\frac{T}{\pi}\right)^{1/2} - \frac{\partial v_k}{\partial x_k}\right] \tag{21}$$

where the deformation rate tensor is

$$S_{ij} = \frac{1}{2}\left(\frac{\partial v_i}{\partial x_j} + \frac{\partial v_j}{\partial x_i}\right) - \frac{1}{3}\frac{\partial v_k}{\partial x_k}\delta_{ij} \tag{21a}$$

and the conductivity of granular temperature is

$$\kappa = 2\rho_p \epsilon_s^2 g_0 d_p (1+e)\left(\frac{T}{\pi}\right)^{1/2} \tag{21b}$$

Then the total stress can be combined in the form

$$\tau_{ij} = \left(-p_s + \epsilon_s \xi_s \frac{\partial v_k}{\partial x_k}\right)\delta_{ij} + 2\epsilon_s \mu_s S_{ij} \tag{22}$$

with the solid phase pressure

$$p_s = \epsilon_s \rho_p [1 + 2(1+e)\epsilon_s g_0] T \tag{22a}$$

the effective solid bulk viscosity

$$\xi_s = \frac{4}{3}\epsilon_s \rho_p d_p g_0 (1+e)\left(\frac{T}{\pi}\right)^{1/2} \tag{22b}$$

and the solid shear viscosity

$$\mu_s = \frac{4}{5}\epsilon_s \rho_p d_p g_0 (1+e)\left(\frac{T}{\pi}\right)^{1/2} \tag{22c}$$

The radial distribution function g_0 proposed by Carnahan and Starling (1969), who derived the g_0 for the dense rigid spherical gases, was used by Savage and Jeffrey (1981), Jenkins and Savage (1983), and Lun et al. (1984). Compared with the simulation results of Alder and Wainright (1960), Figure 1, the values of Carnahan and Starling are lower when ϵ_s is higher than 0.60. The maximum volume fraction of gases may reach 1, but the maximum volume fraction of granules is usually less than 0.7. Our computation shows that the g_0 from Carnahan and Starling gave the solid volume fraction higher than 0.8 at some positions in the fluidized bed. In his later work, Savage (1988) proposed a simple expression for g_0, which is implicit in the work of Bagnold (1954) and was given by Ogawa et al. (1980),

$$g_0 = \left[1 - \left(\frac{\epsilon_s}{\epsilon_{smax}}\right)^{1/3}\right]^{-1} \tag{23}$$

where ϵ_{smax} is the maximum solid volume fraction for a random packing. To match the data of Alder and Wainwright (1960) more closely, we suggest a value of 0.6 multiply the righthand side of Eq. 23. For glass beads of 500 μm dia., we take ϵ_{smax} to be 0.6436. Figure 1 shows g_0 using this ϵ_{smax}.

The collisional stress, given by Eq. 19, and the energy dissipation, given by Eq. 21, are identical to those given by Jenkins and Savage (1983) for their case of $\alpha = 0$.

The solids pressure given by Eq. 22a is similar to the van der Waals equation of state, as shown by Eq. 16.5, 5 in Chapman and Cowling (1970). The kinetic part of the pressure produced proportionality of solids pressure to granular temperature and particle concentration, as in the ideal gas law. The collisional part produced the terms involving the repulsive radial distribution function, which is proportional to the repulsive force due to the finite size of molecules.

It is also instructive to compare the solids shear viscosity given by Eq. 22c to the viscosity of gases obtained from kinetic theory (Chapman and Cowling, 1970). At ordinary pressure the gas viscosity is proportional to the square root of the temperature, as in Eq. 22c. At higher pressure it is divided by a packing function that becomes infinite as the gas approaches the state in which the molecules are packed so closely that motion is impossible, just as in Eq. 22c for the solids.

To examine the behavior of the solids pressure and the solids viscosity as a function of particle volume fraction, it is best to look at the stress in simple shear flow, as done by the developers of the kinetic theory of solids.

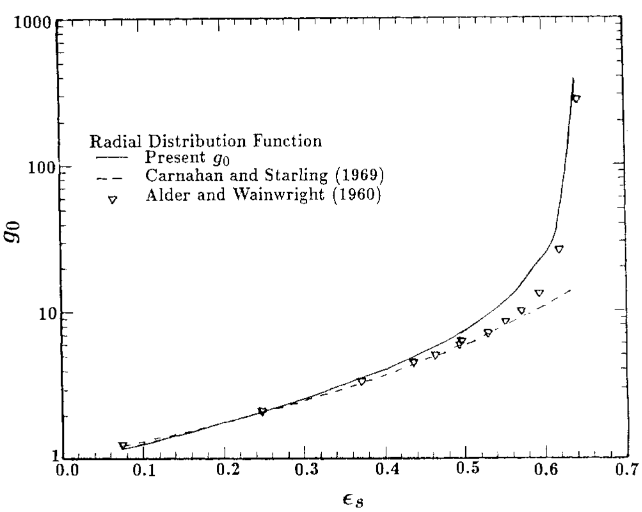

Figure 1. Radial distribution function g_0.

Stresses in simple shear flow

In a simple shear single-phase flow with a uniform granular temperature, the energy equation, Eq. 12, reduces to

$$\tau_{xy}\frac{dv_x}{dy} - \gamma = 0 \tag{24}$$

Substituting the preceding constitutive equations into Eq. 24, we have

$$T = \frac{d_p^2}{5(3-\alpha)}\frac{1}{(1-e)}\left(\frac{dv_x}{dy}\right)^2 \tag{25}$$

where $\alpha = 0$ refers to the present model, and $\alpha = 1$ refers to Jenkins and Savage's (1983) model. This stresses become

$$\tau_{xy} = \frac{4\sqrt{15}}{75\pi^{1/2}}\epsilon_s^2 \rho_p d_p^2 g_0 (1+e)\left(\frac{dv_x}{dy}\right)^2 \tag{26a}$$

$$p_s = \frac{1}{15}\epsilon_s \rho_p d_p^2 [1 + 2\epsilon_s g_0 (1+e)]\frac{1}{(1-e)}\left(\frac{dv_x}{dy}\right)^2 \tag{26b}$$

for the present model, and

$$\tau_{xy} = \frac{3\sqrt{10}}{25\pi^{1/2}} \epsilon_s^2 \rho_p d_p^2 g_0 (1+e) \left(\frac{dv_x}{dy}\right)^2 \quad (27a)$$

$$p_s = \frac{1}{5} \epsilon_s^2 \rho_p d_p^2 g_0 \frac{(1+e)}{(1-e)} \left(\frac{dv_x}{dy}\right)^2 \quad (27b)$$

for the Jenkins and Savage model.

The shear and the normal stress, as well as the experimental data of Savage and Sayed (1984) for 1.5 mm dia., Ballotini glass beads are plotted against ϵ_s and are shown in Figures 2a and 2b, respectively. The coefficient of restitution is assumed to be 0.9. At high solids concentrations, in which the collisional stresses are dominant, the three models are close to each other for both the shear and the normal stresses. At low solids concentrations, in which the collisional stresses are negligible compared with the kinetic stressess, the present model gives a higher normal stress than that of Jenkins and Savage because of the addition of the kinetic part of the normal stress. Both the shear and the normal stresses of Lun et al. (1984) increase with decreasing solids concentration at low solids fractions. This behavior is physically implausible. It causes instabilities, as discussed by Lun et al.

Critical discharge rate

Savage (1988) has shown that his granular flow equations lead to a "sound" speed. In single-phase compressible flow such a sound speed evaluated at a constant entropy is known as the critical velocity. At this condition a reduction in downstream pressure does not result in an increase in the mass flow rate of the fluid. A limit occurs because signals no longer propagate upstream. This limit occurs when the fluid velocity just equals this critical velocity. The theory of partial differential equations shows that information flows along characteristic directions. At the critical conditions one of these characteristics is set to zero. The result is that this critical velocity can be obtained considering the simpler steady-state, one-dimensional equations of change. Hence, consider one-dimensional steady-state two-phase flow. The transport equations with the present constitutive relations reduce themselves to

$$\mathbf{A} \frac{d\mathbf{U}}{dx} = \mathbf{B} \quad (28)$$

where the coefficient matrix $\mathbf{A}$ is

$$\mathbf{A} = \begin{bmatrix} \rho_p v & \epsilon_s \rho_p & 0 & 0 & 0 \\ -\rho_g u & 0 & (1-\epsilon_s)\rho_g & \dfrac{(1-\epsilon_s)u}{U_c^2} & 0 \\ \rho_p \dfrac{d\Gamma}{d\epsilon_s} T & \epsilon_s \rho_p v & 0 & \epsilon_s & \rho_p \Gamma \\ 0 & 0 & (1-\epsilon_s)\rho_g u & (1-\epsilon_s) & 0 \\ 0 & [\Gamma - 3(1-e^2)\epsilon_s^2 g_0]\rho_p T & 0 & 0 & \tfrac{3}{2}\epsilon_s \rho_p v \end{bmatrix} \quad (28a)$$

$$\mathbf{U} = \begin{bmatrix} \epsilon_s \\ v \\ u \\ p \\ T \end{bmatrix} \quad (28b)$$

and

$$\mathbf{B} = \begin{bmatrix} 0 \\ 0 \\ -\epsilon_s \rho_p g + \beta(u - v) - f_{ws} \\ -(1-\epsilon_s)\rho_g g + \beta(v-u) - f_{wg} \\ -12(1-e^2)\epsilon_s^2 \rho_p g_0 T^{3/2}/(\pi^{1/2} d_p) + \epsilon_s \rho_p C_{gs} \end{bmatrix} \quad (28c)$$

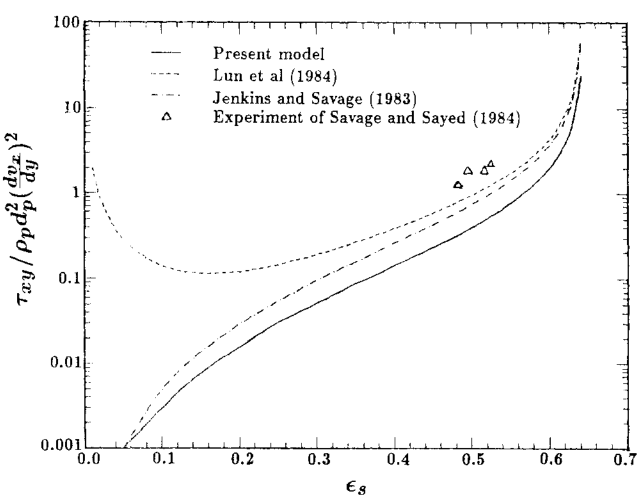

Figure 2a. Nondimensional shear stress vs. solid volume fraction for simple shear flow.

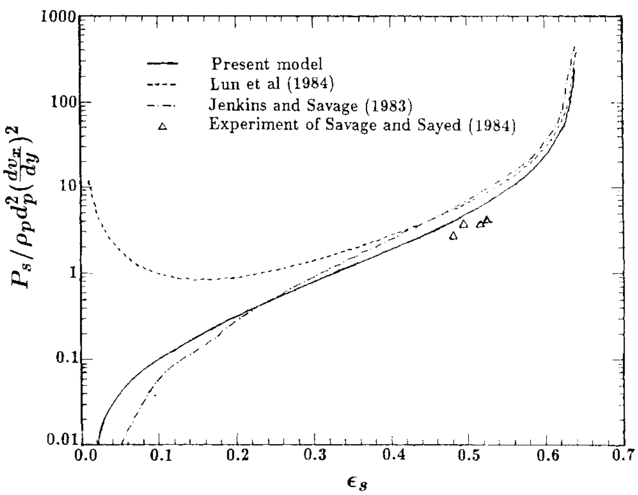

Figure 2b. Nondimensional normal stress vs. solid volume fraction for simple shear flow

and where u and v are the velocities of the gas and the solids, respectively. U_c is the isothermal sound speed of gas equal to $[(\partial p_g/\partial \rho_g)_{T_g}]$. fw is the frictional force on the wall. Γ is a function of ϵ_s and e only,

$$\Gamma = \epsilon_s [1 + 2(1 + e)\epsilon_s g_0] \tag{28d}$$

and

$$C_{gs} = \frac{D}{m} \langle C_{gi} C_i - C_i C_i \rangle \tag{28e}$$

From the condition of critical flow as discussed above (Gidaspow and Syamlal, 1985; Syamlal, 1985),

$$|\mathbf{A}| = 0 \tag{29}$$

we obtain the critical speed of wave propagation, V_c, as

$$V_c = \left[F(\epsilon_s, e)\, T - \frac{\rho_g}{\rho_p} \frac{\epsilon_s}{1 - \epsilon_s} \frac{u^2}{1 - M_g^2} \right]^{1/2} \tag{30}$$

where $M_g = u/U_c$ is the Mach number, and

$$\begin{aligned} F(\epsilon_s, e) = {} & [1 + 2(1 + e)g_0]\,[1 - 2(1 - e^2)\epsilon_s g_0] \\ & + \frac{2}{3}[1 + 2(1 + e)\epsilon_s g_0]^2 \\ & + 2(1 + e)\epsilon_s g_0 \left[1 + \frac{\eta}{3(1 - \eta)}\right] \end{aligned} \tag{30a}$$

$$\eta = \left(\frac{\epsilon_s}{\epsilon_{smax}}\right)^{1/3} \tag{30b}$$

Similar equations can be obtained for the critical velocity by using the constitutive relations of Lun et al. (1984) and Jenkins and Savage (1983). The only difference is in the functions $F(\epsilon_s, e)$, which are

$$\begin{aligned} F(\epsilon_s, e) = {} & [1 + 2(1 + e)g_0] \\ & + \frac{2}{3}[1 + 2(1 + e)\epsilon_s g_0]^2 \\ & + 2(1 + e)\epsilon_s g_0 \left[\frac{\eta}{3(1 - \eta)}\right] \end{aligned} \tag{30c}$$

for Lun's model, and

$$\begin{aligned} F(\epsilon_s, e) = {} & [1 + 2(1 + e)g_0] \\ & [1 - 2(1 - e^2)\epsilon_s g_0] + \frac{8}{3}(1 + e)^2 \epsilon_s^2 g_0^2 \\ & + 2(1 + e)\epsilon_s g_0 \left[1 + \frac{\eta}{3(1 - \eta)}\right] \end{aligned} \tag{30d}$$

for the Jenkins and Savage model.

The effect of the interstitial fluid in Eq. 30 is small and differs from model to model (Gidaspow and Syamlal, 1985). It is not considered further.

If $M_g \ll 1$, and $\rho_g \ll \rho_p$, Eq. 30 reduces to

$$V_c = [F(\epsilon_s, e)\, T]^{1/2} \tag{31}$$

These nondimensional critical velocities $V_c/T^{1/2}$ for the three different constitutive relations with $e = 0.9$ are shown in Figure 3. At high ϵ_s the three models give almost the same values. At low ϵ_s the critical velocity of Jenkins and Savage is lower than others due to the neglect of the kinetic stresses in the model.

Savage (1988) has approximately analyzed the sound speed for single-phase particulate flow using the Jenkins and Savage model. He also roughly estimated V_c by considering a particle moving at its rms fluctuating velocity. He obtained

$$V_c = \frac{1}{1 - \eta}(3T)^{1/2} \tag{32}$$

where 3 occurs due to its definition as $3T = \langle C^2 \rangle$ and the factor involving η is the packing conditions. Equation 32 is also plotted in Figure 3. It gives higher values than does the present analysis. However, it summarizes the essence of the physics. At low packings the critical velocity is simply $\langle C^2 \rangle^{1/2}$. For dilute gas it is of the order of the sonic velocity, 300 m/s. For particulate flow away from maximum packing it is two orders of magnitude lower, as discussed below. At maximum packing the sonic velocity becomes infinite, corresponding to the infinite sonic velocity for propagation through the assumed incompressible solid phase.

In Figure 3, the critical velocity of the previous analysis (Gidaspow and Syamlal, 1985) is plotted against ϵ_s, in which

$$G(\epsilon_s) = \frac{dp_s}{d\epsilon_s} = 10^{8.76\epsilon_s - 0.27} \text{ dyne/cm}^2 \tag{33}$$

Such correlations were based on tilted bed experiments of Rietma and Mutsers (1973), as discussed by Gidaspow (1986). For glass beads, $\rho_p = 2.5$ g/cm^3, $V_c = \sqrt{G/\rho_p} \simeq 1$ m/s at $\epsilon_s \simeq 0.57$. This value is approximately the discharge rate of glass beads from a specially constructed hopper (Gidaspow et al., 1986). The solids volume fraction was measured with an x-ray

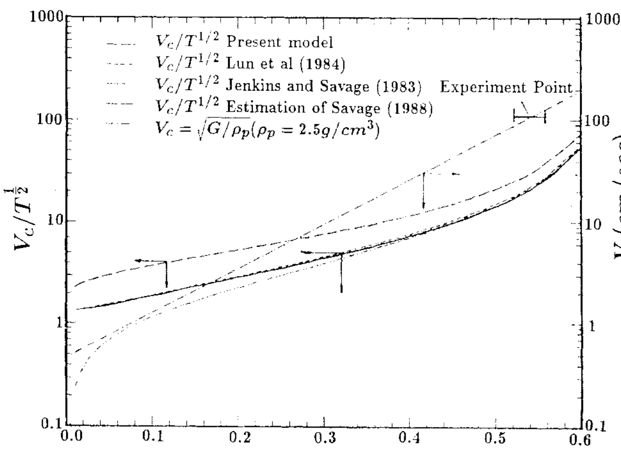

Figure 3. Critical velocity of particulate phase.
Exp.: Gidaspow et al. (1986)

densitometer at the outlet. Such a value of discharge velocities is typical for the height-independent discharge of solids through orifices, as summarized by the correlations given by Cheremisinoff and Cheremisinoff (1984). A complete verification of the granular flow theory must involve the determination of this critical velocity for flow from vessels.

Two-phase Balances and Boundary Conditions

The conservation of mass and momentum equations for each phase and the constitutive relations are given in Table 1. The constitutive equations for the solid derived in this paper and the fluctuating energy equation for the solid phase have been added to our previous computer code (Gidaspow, 1986; Gidaspow and Ettehedieh, 1983). This code generalizes the FLUFIX code (Lyczkowski et al., 1987) used at Argonme National Laboratory for bubbling fluidized bed studies by the addition of this extra granular temperature equation and by the theoretical calculation of the solids pressure and solids viscosity. Our computer code using the ICE numerical method for two-phase flow (Harlow and Amsden, 1975; Rivard and Torrey, 1977) has been demonstrated to be adaptable to a variety of problems (Gidaspow, 1986; Symlal, 1985; Ding, 1990).

To solve the equations of gas-solids flow listed in Table 1, we need appropriate boundary conditions for velocities of the solids and the gas, for gas phase pressure, and for granular temperature. The porosity is set to 1 where particle-free gas enters the system. At an impenetrable solid wall, the gas phase velocities in the two directions are generally set to zero. This no-slip condition cannot always be applied to solid motion. Since the particle diameter is usually larger than the length scale of surface roughness of the rigid wall, the particles may partially slip at the wall. According to the assumption of Eldighidy et al. (1977) that the solid tangential velocity v_{s2} at the wall is proportional to its gradient at the wall, we can write

$$v_{s2}\,|_w = -\lambda_p \frac{\partial v_{s2}}{\partial x_1}\Big|_w \tag{34}$$

where the x_1 direction is normal to the wall. We let the slip parameter λ_p be the mean distance between particles. λ_p can be

Table 1. Governing Equations for Gas-Solid Flow

1. Continuity Equation for Phase k ($= g, s$)

$$\frac{\partial}{\partial t}(\epsilon_k \rho_k) + \nabla \cdot (\epsilon_k \rho_k \mathbf{v_k}) = 0 \tag{T1}$$

2. Momentum Equation for Phase k($= g, s$)

$$\frac{\partial}{\partial t}(\epsilon_k \rho_k \mathbf{v_k}) + \nabla \cdot (\epsilon_k \rho_k \mathbf{v_k v_k}) = -\epsilon_k \nabla p_g + \epsilon_k \rho_k \mathbf{g} + \nabla \cdot \bar{\bar{\tau}}_\mathbf{k} + \beta(\mathbf{v_l} - \mathbf{v_k}) \tag{T2}$$

3. Gas Phase Stress

$$\bar{\bar{\tau}}_\mathbf{g} = 2\epsilon_g \mu_g \bar{\bar{\mathbf{S}}}_\mathbf{g} \tag{T3}$$

where

$$\bar{\bar{\mathbf{S}}}_\mathbf{g} = \tfrac{1}{2}[\nabla \mathbf{v_g} + (\nabla \mathbf{v_g})^T] - \tfrac{1}{3}\nabla \cdot \mathbf{v_g} \bar{\bar{\mathbf{I}}} \tag{T3a}$$

4. Solid Phase Stress

$$\bar{\bar{\tau}}_\mathbf{s} = [-p_s + \epsilon_s \xi_s \nabla \cdot \mathbf{v_s}]\bar{\bar{\mathbf{I}}} - 2\epsilon_s \mu_s \bar{\bar{\mathbf{S}}}_\mathbf{s} \tag{T4}$$

Deformation rate

$$\bar{\bar{\mathbf{S}}}_\mathbf{s} = \tfrac{1}{2}[\nabla \mathbf{v_s} + (\nabla \mathbf{v_s})^T] - \tfrac{1}{3}\nabla \cdot \mathbf{v_g} \bar{\bar{\mathbf{I}}} \tag{T4a}$$

Solid phase pressure

$$p_s = \epsilon_s \rho_p [1 + 2(1+e)\epsilon_s g_0] T \tag{T4b}$$

Solid phase bulk viscosity

$$\xi_s = \frac{4}{3}\epsilon_s \rho_p d_p g_0 (1+e)\left(\frac{T}{\pi}\right)^{1/2} \tag{T4c}$$

Solid phase shear viscosity

$$\mu_s = \frac{4}{5}\epsilon_s \rho_p d_p g_0 (1+e)\left(\frac{T}{\pi}\right)^{1/2} \tag{T4d}$$

Radial distribution function

$$g_0 = \frac{3}{5}\left[1 - \left(\frac{\epsilon_s}{\epsilon_{smax}}\right)^{1/3}\right]^{-1} \tag{T4e}$$

Fluctuating energy $\tfrac{3}{2}T$ ($= \tfrac{1}{2}\langle C^2 \rangle$) equation

$$\frac{3}{2}\left[\frac{\partial}{\partial t}(\epsilon_s \rho_p T) + \nabla \cdot (\epsilon_s \rho_p \mathbf{v_s} T)\right] = \bar{\bar{\tau}}_\mathbf{s} : \nabla \mathbf{v_s} - \nabla \cdot \mathbf{q} - \gamma - 3\beta T \tag{T5}$$

Collisonal energy dissipation γ

$$\gamma = 3(1 - e^2)\epsilon_s^2 \rho_p g_0 T\left[\frac{4}{d_p}\left(\frac{T}{\pi}\right)^{1/2} - \nabla \cdot \mathbf{v_s}\right] \tag{T5a}$$

Flux of fluctuating energy $\mathbf{q}$

$$\mathbf{q} = -\kappa \nabla T \tag{T5b}$$

Conductivity of the fluctuating energy

$$\kappa = 2\rho_p \epsilon_s^2 d_p (1+e) g_0 \left(\frac{T}{\pi}\right)^{1/2} \tag{T5c}$$

5. Gas-Solid Drag Coefficients for $\epsilon < 0.8$, (based on Ergun equation)

$$\beta = 150\frac{\epsilon_s^2 \mu_g}{\epsilon d_p^2} + 1.75\frac{\rho_g \epsilon_s |\mathbf{v_g} - \mathbf{v_s}|}{d_p} \tag{T6}$$

for $\epsilon \geq 0.8$, (based on empirical correlation)

$$\beta = \frac{3}{4} C_d \frac{\epsilon \epsilon_s \rho_g |\mathbf{v_g} - \mathbf{v_s}|}{d_p} \epsilon^{-2.65} \tag{T7}$$

where

$$C_d = \frac{24}{R_{ep}}[1 + 0.15(R_{ep})^{0.687}], \quad \text{for} \quad R_{ep} < 1{,}000 \tag{T8a}$$

$$C_d = 0.44, \quad \text{for} \quad R_{ep} \geq 1{,}000 \tag{T8b}$$

$$R_{ep} = \frac{\epsilon \rho_g |\mathbf{v_q} - \mathbf{v_s}| d_p}{\mu_g} \tag{T8c}$$

estimated by

$$\epsilon_s \frac{4}{3}\pi\left(\frac{\lambda_p}{2}\right)^3 = \frac{\pi}{6} d_p^3$$

to obtain

$$\lambda_p = \frac{1}{\epsilon_s^{1/3}} d_p \tag{35}$$

Note that for small particle diameters the boundary condition is close to the no-slip condition.

The boundary condition for solid velocity at the wall derived by Hui et al. (1984) is similar to Eq. 34. Their slip parameter λ_p is proportional to particle diameter and is the inverse of the wall roughness parameter. Jenkins' boundary conditions (Mastorakos et al., 1988) is also in the form of Eq. 34. His slip parameter is proportional to particle diameter and is a function of solid volume fraction. A comparison of Eq. 35 and Jenkins' theory is shown in Figure 4. For $\epsilon_s > 0.2$, the difference is small. For $\epsilon_s < 0.2$, Jenkins' theory gives a higher slip parameter than Eq. 35, but both tend to infinity when $\epsilon_s \rightarrow 0$.

The boundary conditons for granular temperature or granular thermal velocity derived by Jenkins (Mastorakos et al., 1988) and Hui et al. (1984) are in the form of Eq. 34. In their boundary condition for granular temperature, the coefficient of restitution of the particle-wall collisions is included. Johnson and Jackson (1987) derived the boundary condition for fluctuating energy by equating the energy flux to the energy dissipation due to the inelastic collision between particles and wall, and energy generation due to the particle slip at the wall. In the following computation, we simply assume the energy flux at the wall to be zero.

The boundary conditions at the symmetric axis demand that gradient of all variables be zero. The inlet conditions for the fluidized bed are given. At the outlet, the pressure is at an ambient atmosphere and the mass flux is assumed to be continuous. Initially, the fluidized bed is at a minimum fluidization, as in other related studies (Gidaspow, 1986).

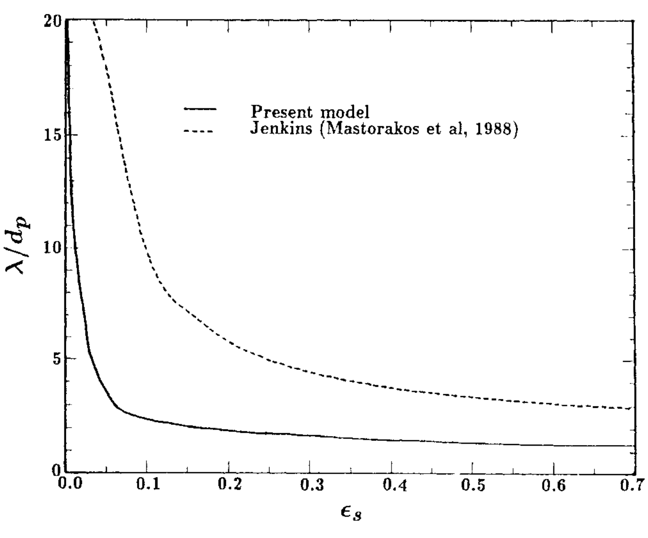

Figure 4. Slip parameter at solid wall vs. solid volume fraction.

Computed Results

Computation with an obstacle

As a part of a cooperative research and development venture on erosion of fluidized-bed combustor heat transfer tubes conducted at Argonne National Laboratory, several simplified geometries roughly representing tubes in a combustor were chosen for simulation and experimental studies. The first geometry chosen was an obstacle placed into a two-dimensional fluidized bed with a jet, as full described by Bouillard et al. (1989a, b). The simulation was done using two inviscid models (Bouillard et al., 1989a) and with a model in which the solids viscosity was varied (Bouillard et al., 1989b). The two inviscid models and a model with a solids viscosity of 0.1 Pa·s produced time-averaged porosities in agreement with the experiment at IIT. Bubble sizes and frequency as determined from high-speed movies were in a rough agreement with the experiment, with the marked difference caused by a strong asymmetry observed in the experiment. The computed porosity oscillations, however, in all three cases showed a disturbing slow decrease of amplitude with time. Since at publication time no experimental porosity oscillations were available for comparison with the theories, these observations were dismissed as perhaps unavoidable damping caused by numerics. Now porosity and pressure oscillations have been systematically measured as a part of the erosion venture for the geometry under consideration and for other configurations. The porosity oscillations were measured using the gamma ray densitometer used by Seo, as described by Gidaspow (1986),

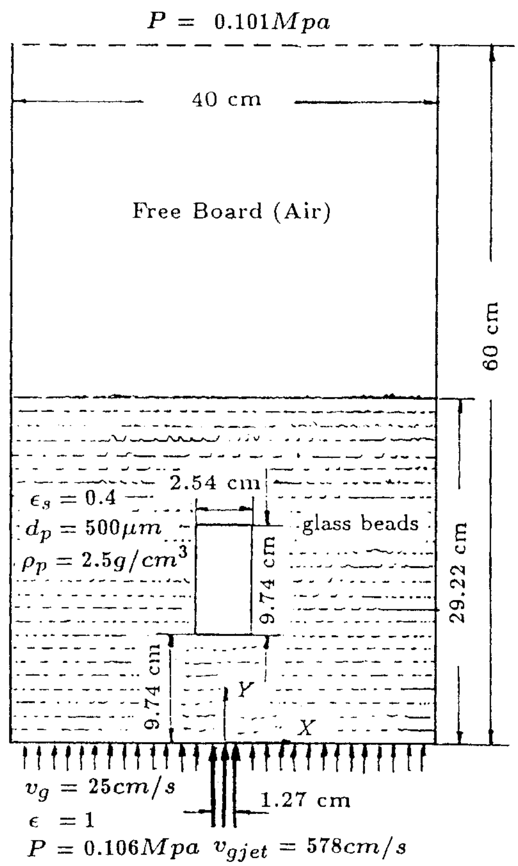

Figure 5. Two-dimensional bed with conditions used in experiment and in computation.

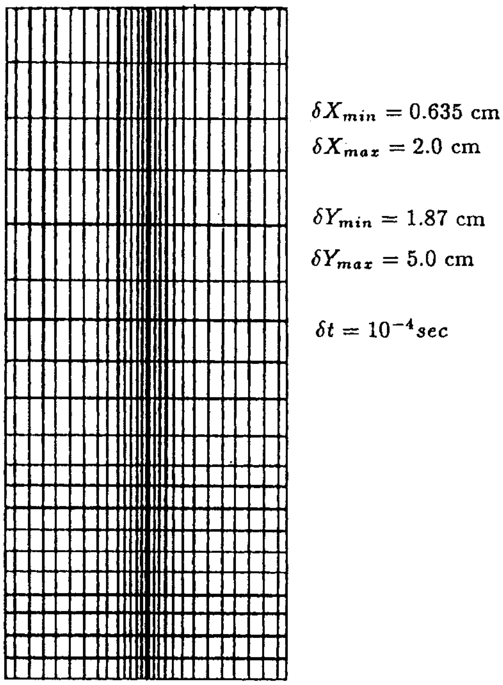

Figure 6. Finite-difference grids used in simulation with an obstacle (16 × 22 nodes).

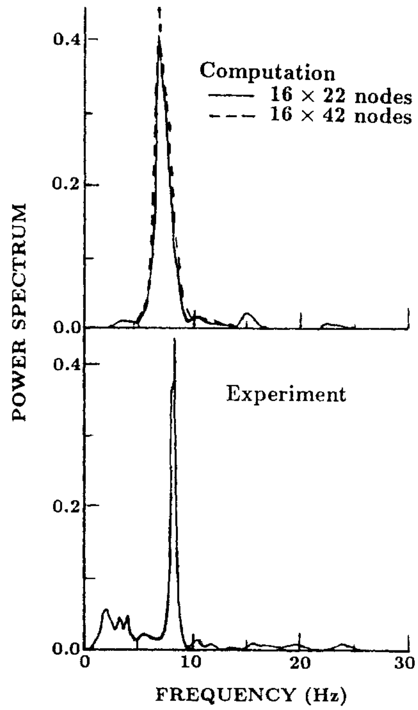

Figure 7b. Computed and experimental power spectrum of porosity oscillation near jet opening.

except that a spectral analysis program was used in conjunction with an IBM PC computer to analyze the data (Gidaspow et al., 1988). In view of the availability of the new data, a closer comparison of the theories to the experiment is now possible.

Figure 5 shows a sketch of the experiment, with a symmetry of the conditions used in the experiment and in the simulation. They are those given by Bouillard et al. (1989a). Nonuniform finite-difference grids used in the computation with cell number 16 × 22, 16 in the x direction and 22 in y direction, are shown in Figure 6. To check the influence of the grid size on the computed results, a finer mesh was utilized in the computation. The same number and size of the computational cells in the x direction were used, but the size in the y direction was half of the previous grid size. The total number of the finer cells is 16 × 42. The time step for the finer mesh was 5×10^{-5} s. The symmetry assumption was made. The computations were continued to 5 s of real time.

Figures 7a and 7b show a comparison of computed and experimental instantaneous porosities at the point $X = 0.31$, $Y = 1.0$ cm, where X is the horizontal coordinate starting from the bed center and Y is the vertical coordinate starting from the bed bottom. The computed amplitude of the porosity oscillation is similar to the experimental result. A spectral analysis of the computed results with 16 × 22 nodes and 16 × 42 nodes gives an

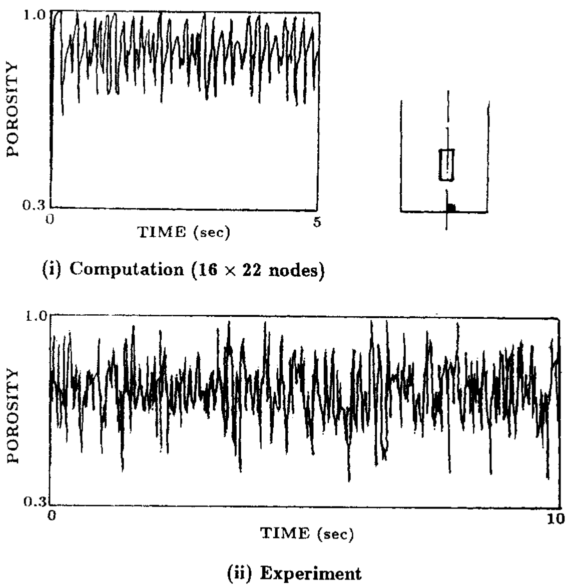

Figure 7a. Computed and experimental porosity oscillation near jet opening (computer with 16 × 22 nodes).

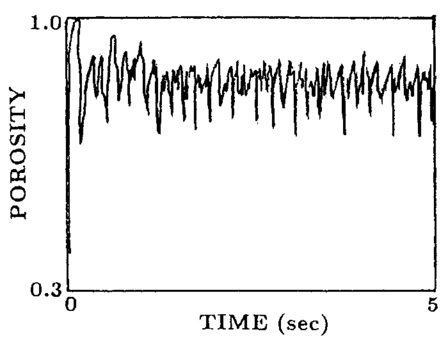

Figure 7c. Computed porosity oscillation near jet opening by model of Jenkins and Savage (1983) (computed with 16 × 22 nodes).

oscillation frequency of about 6 Hz, while the experiment gives 8 Hz. The higher experimental frequency is probably due to the neglect of the wall effect in the model. Figure 7c shows the computed porosity with the model of Jenkins and Savage (1983) at the same point. It gave incorrect amplitude of porosity oscillation. Therefore, we do not use the Jenkins and Savage model for the simulation of bubbling fluidization. The experimental bubbling frequency on the left side of the obstacle ($X = 1.6$ cm) is about 3 Hz. It is lower than the computed frequency of about 5.5 Hz, as shown in Figure 8b. The reason may be due to the asymmetrical effect observed in the experiment. Figure 2 in Bouillard et al. (1989a) clearly shows the asymmetry in the experiment. A comparison of computed frequencies of porosity oscillations with the experiment at a point below the obstacle is shown in Figure 9. The agreement between the computations using 16×22 nodes and 16×42 nodes is good, as can be seen from Figures 7b, 8, and 9.

The computed results with the present model are compared with that of the previous inviscid model computed by Bouillard and coworkers (Bouillard, 1986; Bouillard et al, 1989a). Figure 10 shows the computed porosity oscillation on the side of the obstacle obtained by Bouillard (1986). The present computation using the kinetic theory model gives a correct pattern of porosity oscillation while the previous model gave a damping of the amplitude of porosity oscillation with time.

Figure 11 shows the time-averaged porosity as a function of bed height at 10 cm from center. An excellent agreement between the present computations of two different node meshes and the experiment was found.

Figure 12 shows the computed bubble evolution at several later times. A bubble forms near the jet opening, propagates around the obstacle, and finally bursts at the top of the bed. The rectangular features in the computed particle distributions are due to the large grid sizes used away from the obstacle.

Figure 13 shows the computed time-averaged solids viscosity in the bed. Although the solids viscosity varies with the position in the bed, its numerical value is not too far from the assumed solids viscosity used in the computations of Bouillard et al.

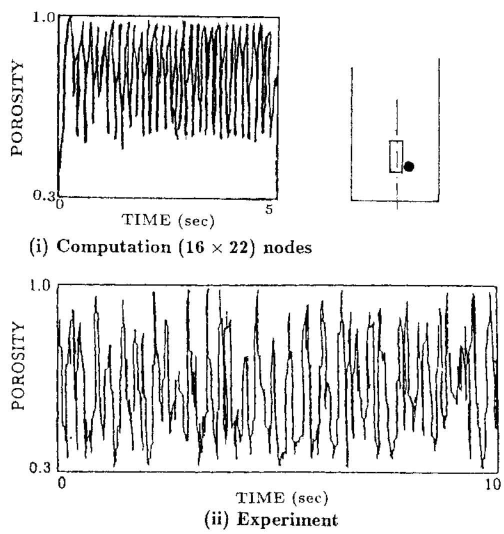

Figure 8a. Computed and experimental porosity oscillation on left side of obstacle, at point of $X = 1.6$, $Y = 11$ cm.

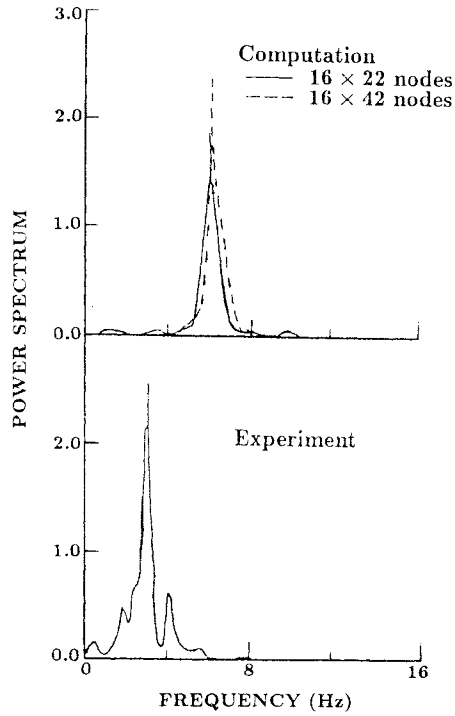

Figure 8b. Computed and experimental power spectrum of porosity oscillation at point of $X = 1.6$, $Y = 11$ cm.

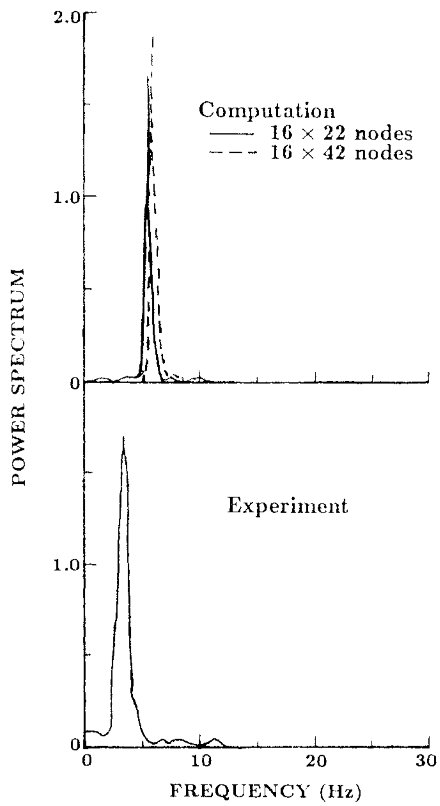

Figure 9. Computed and experimental power spectrum of porosity oscillation below obstacle, at point of $X = 0.3$, $Y = 8.8$ cm.

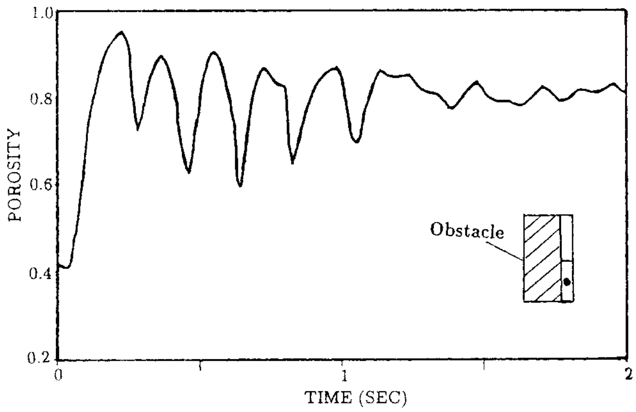

Figure 10. Computed porosity oscillation on side of obstacle by Bouillard (1986) (compared with Figure 8a).

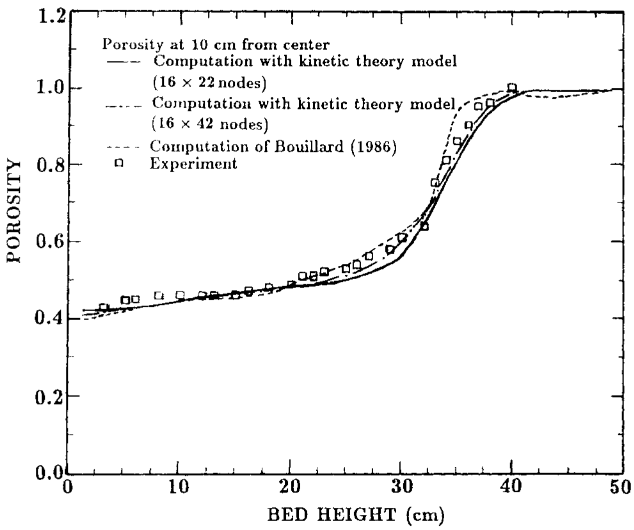

Figure 11. Comparison of present computed time-averaged porosity as a function of bed height at 10 cm from center with experiment and previous computed data of Bouillard et al. (1989a).

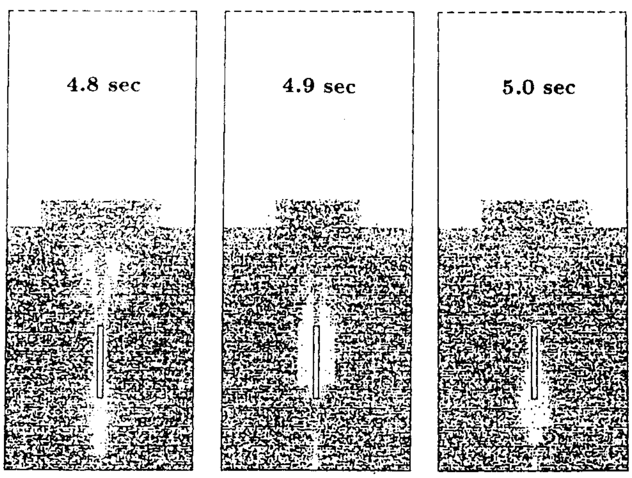

Figure 12. Computed bubbles in bed with an obstacle at several later times (16 × 22 nodes).

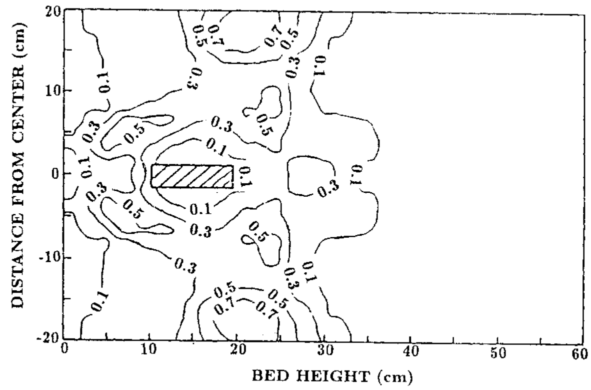

Figure 13. Computed time-averaged solid viscosity (Pa · s) in bed with an obstacle (16 × 22 nodes).

(1989b). The key point is that this viscosity need not be guessed any more. It is automatically computed, and so is the value of the solids stress. There is no need to vary it parametrically, as done previously by Bouillard et al. (1989a). The time-averaged granular temperature around the obstacle in which the solid shear rate is generally high is shown in Figure 14. The granular temperature is high wherever there is a great deal of motion. It shows that a typical value of the fluctuating velocity is of the order of 10 cm/s, in rough agreement with the critical discharge velocity.

Computation for uniform fluidization

The computations were repeated for the case of fluidization with a uniform inlet velocity. The case of uniform fluidization is a good test case of this kinetic theory model.

The computation has been compared with the experimental results of Lin et al. (1985), who measured particle velocity in a cylindrical bed using a unique radioactive particle tracking

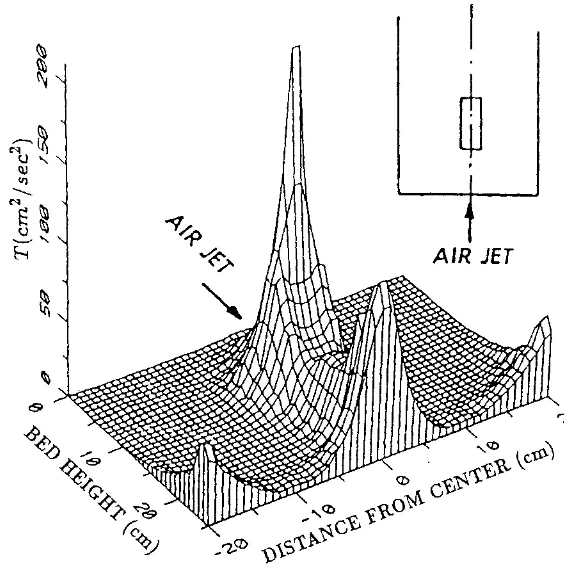

Figure 14. Computed time-averaged granular temperature T around obstacle where $3T = \langle C^2 \rangle$ (16 × 22 nodes).

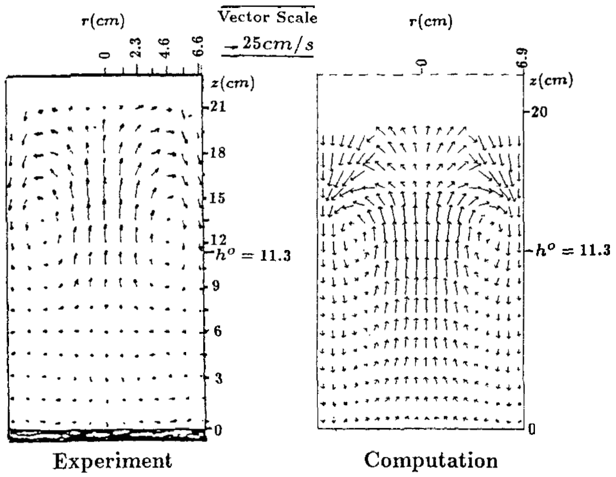

Figure 15. Experimental and computed solids velocities in cylindrical bed, inlet air velocity 64.1 cm/s
Exp.: Lin et al (1985)

method. The cylindrical bed, 13.8 cm dia., contains 420–600 μm dia. glass beads, with a static bed height of 11.3 cm. In the computation, we took a particle diameter of 500 μm and a particle density of 2.5 g/cm^3. Uniform grid sizes were used. These were $\Delta r = 0.69$ cm and $\Delta z = 1.13$ cm. The time step was $\Delta t = 10^{-5}$ s. Figure 15 shows the agreement between the computed time-average solids flow pattern and measured data for a superficial fluidization velocity, $U_0 = 64.1$ cm/s. The particles ascend at the center and descend near the wall. A vortex appeared in the upper portion between the center and the wall. Such flow pattern is related to the bubble motion. Figure 16 shows the computed particle distributions at several times. The bubbles tend to move toward the bed center and finally merge at the center. This bubble motion behavior has been

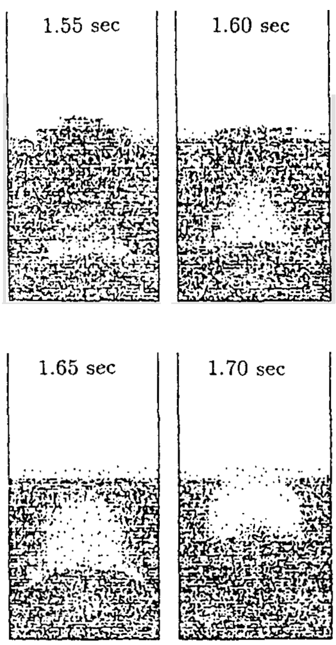

Figure 16. Computed bubbles in cylindrical bed at several times, inlet air velocity 64.1 cm/s.

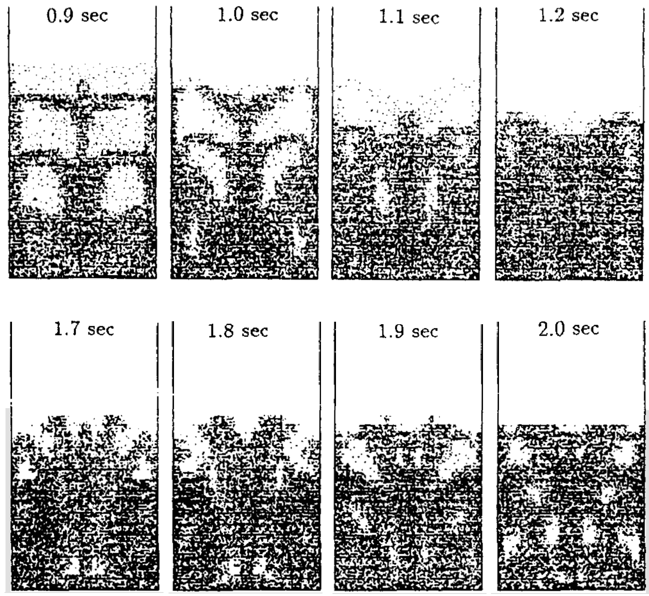

Figure 17. Computed bubbles in rectangular two-dimensional bed, uniform inlet air velocity 100 cm/s.

reported by Werther and Molerus (1973). Hence, the higher solids velocity in the upper portion of the bed center is due to the bubble coalescence and bubble motion.

Another test case for the kinetic theory model is the simulation of the uniform fluidization in the IIT rectangular two-dimensional bed with an inlet air velocity of 100 cm/s. This velocity is about four times the minimum fluidization velocity of glass beads of 500 μm dia. and 2.5 g/cm^3 density. The initial static bed height is 29.94 cm. The dimensions of the bed are the same as those shown in Figure 5. Figure 17 shows the computed particle distributions at several times in the two-dimensional bed. Bubbles form between the bed center and the bed wall.

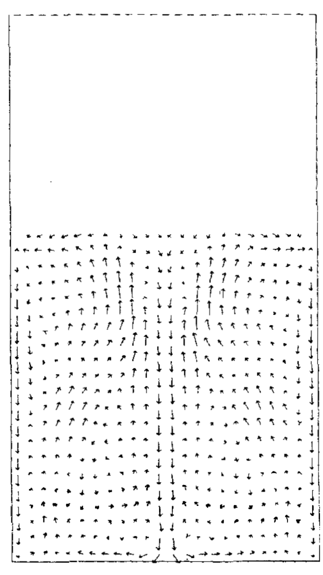

Figure 18. Computed time-averaged solids flow pattern in rectangular two-dimensional bed, uniform inlet air velocity of 100 cm/s.

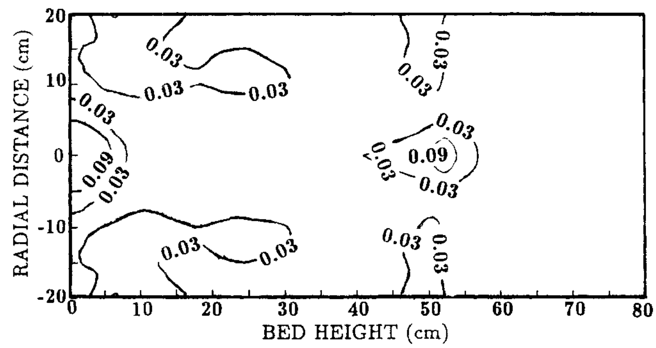

Figure 19. Time-averaged solids viscosity (Pa · s) in rectangular two-dimensional bed, uniform inlet air velocity 100 cm/s.

They move to the bed center but burst before merging. There is a downward motion of the particles at center of the bed and at the walls of the bed, as shown in Figure 18. The computed solids viscosities are between 0.03 and 0.1 Pa · s, as shown in Figure 19. Figure 20 shows high fluctuating energy in the top portion of the bed. We expect a high fluctuating intensity of the particles in this region. An experiment in progress for the uniform fluidization in the rectangular two-dimensional bed shows that the computed bubbles and the flow pattern agree with observations.

The observed and the computed bubble formation for uniform fluidization can be explained on the basis of a simplified version of the hydrodynamic model. A simplified analysis of the type used in the free convection single-phase flow shows that in the absence of viscosity the rate of change of solids vorticity, ζ, can

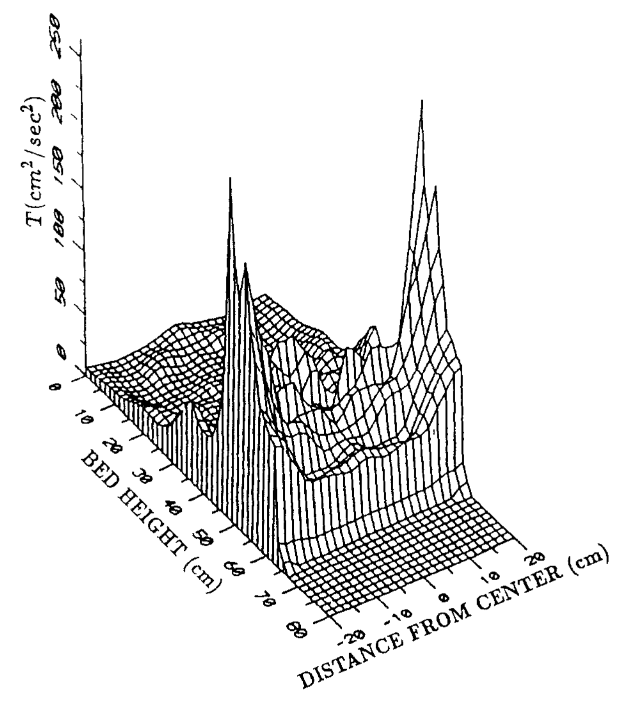

Figure 20. Time-averaged granular temperature in rectangular two-dimensional bed, uniform inlet air velocity 100 cm/s.

be related to the gradient of porosity, as follows,

$$\frac{d\zeta}{dt^s} = -\frac{g}{(1-\epsilon_{mf})}\frac{\partial\epsilon}{\partial y} \tag{36}$$

where ϵ_{mf} is the porosity at minimum fluidization. Downward particle motion at the eall sets up the circulation or vorticity. This solids vorticity then gives rise to the vertical porosity gradient, as shown by the above equation. A nonuniform porosity gradient at the bottom of the bed causes nonuniform void propagation. For Geldart type B particles the void moves faster in the dilute region. There is a catch-up effect, an intersection of void paths. Hence bubbles form in the region between the walls and the center of the bed, as shown in the flow patterns in Figures 15 and 18. The angle that the bubbles make with the horizontal depends on the fluid velocity, the height of the bed, and the geometry. In the case of fluidization with a jet, the bubble always forms at the jet. A strength of the present model is that it can correctly predict bubbling fluidization with a uniform injection velocity.

Conclusions

1. A predictive two-phase flow model was derived starting with the Boltzmann equation for velocity distribution of particles using previous kinetic theory of granular flow. The model was shown to compute reasonable solids viscosities, repulsive solids stresses, and critical discharge velocities.

2. The model correctly predicted the experimentally measured time-averaged porosities in two-dimensional fluidized beds. It predicted porosity oscillations that agreed with experiments better than previous models. It predicted the formation of bubbles and solids flow pattern for fluidization with a uniform inlet velocity in agreement with measurement and observations.

Acknowledgment

This study was partially supported by a grant from the National Science Foundation, "Hydrodynamics of Fluidization and Segregation," as a part of an industry-university cooperative program with EXXON Research and Engineering. The authors thank the EXXON Education Foundation for partial support of this work. The application to fluidized bed combustors was supported by a grant from the Argonne National Laboratory as a part of the R&D venture "Erosion of FBC Heat Transfer Tubes," and NCSA University of Illinois Cray X-MP was used.

Notation

$\mathbf{A}$ = coefficient matrix, Eq. 28a
$\mathbf{B}$ = matrix, Eq. 28c
C = fluctuating velocity of particle
C_d = drag coefficient
C_{gs} = correlation of two phases, Eq. 28e
$\mathbf{c}$ = instaneous velocity of a particle
$\mathbf{c}_{12}$ = relative velocity of particle 1 and 2
D = drag force coefficent
d_p = particle diameter
e = coefficient of restitution
F = external force per unit mass acting on a particle
f = single-particle velocity distribution function
f^2 = pair-distribution function
G = modulus of solid phase
g = gravity
g_0 = radial distribution function
$\bar{\mathbf{I}}$ = unit tensor
k = unit vector along the line from center of particle 1 to 2
M_g = Mach number

m = particle mass
n = particle number density
p = pressure
$\mathbf{q}$ = flux vector of fluctuating energy
$\mathbf{r}$ = space vector
$\overline{\overline{S}}$ = deformation rate
$3/2T$ = fluctuating energy
t = time
U = matrix, Eq. 28b
u = gas mean velocity
v = solid mean velocity
x, y = rectangular coordinate

Greek letters

α = parameters in Jenkins and Savage model
β = two-phase drag coefficient
Γ = function of ϵ_s and e, Eq. 28d
γ = collisional energy dissipation
ϵ, ϵ_s = gas and solid volume fraction
ϵ_{mf} = porosity at minimum fluidization
ζ = solids vorticity
η = defined in Eq. 30b
$\boldsymbol{\Theta}$ = defined in Eq. 8a
κ = conductivity of granular temperature
λ_p = mean distance between particles
μ = shear viscosity
ξ = bulk viscosity
ρ = density
τ = stress
ϕ_c = collisional rate of change
χ = defined in Eq. 8b
ψ = single-particle quantity

Subscripts

g = gas phase
s = solid phase
i = vector component of i
ij = tensor component of ij
j = vector component of j
k = vector component of k
x = vector component in x direction
y = vector component in y direction
1, 2 = particle 1, 2 or vector component 1, 2

Superscripts

c = collisional part
k = kinetic part

Literature Cited

Avidan, A. A., M. Edwards, and H. Owen, "Fluid Catalytic Cracking—Past and Future Challenges," *Sixth Int. Conf. Fluidization*, Banff, Alberta, Canada (1989).

Alder, B. J., and T. E. Wainwright, "Studies in Molecular Dynamics. II: Behavior of a Small Number of Elastic Spheres," *J. Chem. Phys.*, **33**, 1439 (1960).

Bagnold, R. A., "Experiments on a Gravity-Free Dispersion of Large Solid Spheres in a Newtonian Fluid under Shear," *Proc. Roy. Soc.*, **A225**, 49 (1954).

Bouillard, J. X., "Hydrodynamics of Sedimentation, Fluidization and Erosion," Ph.D. Thesis, Illinois Inst. Technol., Chicago (1986).

Bouillard, J. X., R. W. Lyczkowski, and D. Gidaspow, "Porosity Distributions in a Fluidized Bed with an Immersed Obstacle," *AIChE J*, **35**(6), 908 (1989a).

Bouillard, J. X., R. W. Lyczkowski, S. Folga, D. Gidaspow, and G. F. Berry, "Hydrodynamics of Erosion of Heat Exchanger Tubes in Fluidized Bed Combustors," *Canad. J. Chem. Eng.*, **67**, 218 (1989b).

Carnahan, N. F., and K. E. Starling, "Equation of State for Nonattracting Rigid Spheres," *J. Chem. Phys.*, **51**, 635 (1969).

Chapman, S., and T. G. Cowling, *The Mathematical Theory of Non-Uniform Gases*, 3rd ed., Cambridge Univ. Press (1970).

Cheremisinoff, N. P., and P. N. Cheremisinoff, *Hydrodynamics of Gas-Solids Fluidization*, Gulf Pub. Co., Houston, TX (1984).

Ding, J., "A Fluidization Model Using Kinetic Theory of Granular Flow," Ph.D. Thesis, Illinois Inst. Technol., Chicago (1990).

Eldighidy, S. M., R. Y. Chen, and R. A. Comparin, (1977). "Deposition of Suspensions in the Entrance of a Channel," *J. Fluid Eng., Trans. ASME*, June, 365 (1977).

Ettehadieh, B., D. Gidaspow, and R. W. Lyczcowski, "Hydrodynamics of Fluidization in a Semicircular Bed with a Jet," *AIChE J.*, **30**, 529 (1984).

Garg, S. K., and J. W. Pritchett, "Dynamics of Gas-Fluidized Beds," *J. Appl. Phys.*, **46**, 4493, (1975).

Gidaspow, D., "Hydrodynamics of Fluidization and Heat Transfer: Supercomputer Modeling," *Appl. Mech. Rev.*, **39**(1), (1986).

Gidaspow, D., and B. Ettehadieh, "Fluidization in Two-Dimensional Beds with a Jet. II: Hydrodynamic Modeling," *Ind. Eng. Chem. Fundam.*, **22**, 193 (1983).

Gidaspow, D., and M. Syamlal, "Solid-Gas Critical Flow," *Ann. Meet. AIChE*, (1985).

Gidaspow, D., Y. C. Seo, and B. Ettehadieh, "Hydrodynamics of Fluidization: Experimental and Theoretical Bubble Sizes in a Two-Dimensional Bed with a Jet," *Chem. Eng. Comm.*, **22**, 253 (1983a).

———, "Hydrodynamics of Fluidization Effect of Pressure," Paper presented at Fine Particles Soc. Meet. (1983b).

Gidaspow, D., J. Ding, and K.-M. Luo, "A Measurement of the Modulus of Elasticity Using Critical Flow Theory," DOE Report DE86011993 (April, 1986).

Gidaspow, D., Y.-P. Tsuo, J. Ding, and I. Gamwo, "Two-Dimensional Fluidized Bed Experiment," *First Quarter Report to Argonne National Laboratory* (Nov., 1988).

Harlow, F. H., and A. A. Amsden, "Numerical Calculation of Multiphase Fluid Flow," *J. Comput. Phys.*, **17**, 19 (1975).

Hui, K., P. K. Haff, J. E. Ungar, and R. Jackson, "Boundary Conditions for High-Shear Grain Flows," *J. Fluid Mech.*, **145**, 223 (1984).

Jenkins, J. T., and S. B. Savage, "A Theory for the Rapid Flow of Identical, Smooth, Nearly Elastic Spherical Particles," *J. Fluid Mech.*, **130**, 187 (1983).

Jackson, R., "The Mechanics of Fluidized Beds," *Trans. Inst. Chem. Eng.*, **41**, (1963).

———, "Hydrodynamic Stability of Fluid-Particle Systems," *Fluidization*, J. F. Davidson, R. Clift, D. Harrison, eds., Academic Press, 47 (1985).

Johnson, P. C., and R. Jackson, "Frictional-Collisional Constitutive Relations for Granular Materials with Application to Plane Shearing," *J. Fluid Mech.*, **176**, 67 (1987).

Lin, J. S., M. M. Chen, and B. T. Chao, "A Novel Radioactive Particle Tracking Facility for Measurement of Solids Motion in Gas-Fluidized Beds," *AIChE J.*, **31**(3), 465 (1985).

Lun, C. K. K., S. B. Savage, D. J. Jeffrey, and N. Chepurniy, "Kinetic Theories for Granular Flow: Inelastic Particles in Couette Flow and Slightly Inelastic Particles in a General Flow Field," *J. Fluid Mech.*, **140**, 223 (1984).

Lyczkowski, R. W., J. X. Bouillard, G. F. Berry, and D. Gidaspow, "Erosion Calculations in a Two-Dimensional Fluidized Bed," *Int. Conf. on Fluidized-Bed Combustion*, **2**, J. P. Mustonen, ed., *ASME*, 697 (1987).

Mastorakos, E., M. Louge, and J. T. Jenkins, "The Role of Particle Collisions in Pneumatic Transport," *Ann. Meet. AIChE*, (1988).

Ogawa, S., A. Umemura, and N. Oshima, "On the Equations of Fully Fluidized Granular Materials," *J. Appl. Math. Phys.*, **31**, 483 (1980).

Pourahmadi, F., and A. C. Humphrey, "Modeling Solid-Fluid Turbulent Flows with Application to Predicting Erosive Wear," *Physico-Chemical Hydrodynamics*, **4**(3), 191 (1983).

Rietma, K., and S. M. P. Mutsers, "The Effect of Interparticle Forces on Expansion of a Homogeneous Gas-Fluidized Bed," *Proc. Int. Symp. Fluidization*, Toulouse, France, 32 (1973).

Rivard, W. C., and M. D. Torrey, "K-FIX: A Computer Program for Transient Two-Dimensional, Two-Fluid Flow," *LA-NUREG-6623*, Los Alamos (1977).

Savage, S. B., "Granular Flows at High Shear Rates," *Theory of Dispersed Multiphase Flow*, R. E. Meyer, ed., Academic Press, 339 (1983)

———, "Streaming Motions in a Bed of Vibrationally Fluidized Dry Granular Material," *J. Fluid Mech.*, **194**, 457 (1988).

Savage, S. B., and D. J. Jeffrey, (1981). "The Stress Tensor in a Granular Flow at High Shear Rates," *J. Fluid Mech.*, **110**, 255 (1981).

Savage, S. B., and M. Sayed, "Stresses Developed by Dry Cohesionless Granular Materials Sheared in an Annular Shear Cell," *J. Fluid. Mech.*, **142**, 391 (1984).

Shahinpoor, M., and G. Ahmadi, "A Kinetic Theory for the Rapid Flow of Rough Identical Spherical Particles and the Evolution of Fluctuation," *Advances in the Mechanics and the Flow of Granular Materials*, II, M. Shahinpoor, ed., *Trans. Tech. Pub.*, Andermannsdorf, Switzerland, 641 (1983).

Soo, S. L., *Fluid Dynamics of Multiphase System*, Blaisdell, Waltham, MA (1967).

Squires, A. M., M. Kwauk, and A. A. Avidan, "Fluid Beds: At Last, Challenging Two Entrenched Practices," *Science*, **230**(4732), 1329 (1985).

Syamlal, M., "Multiphase Hydrodynamics of Gas-Solids Flow," Ph.D. Thesis, Illinois Inst. Technol., Chicago (1985).

Syamlal, M., and D. Gidaspow, "Hydrodynamics of Fluidization: Prediction of Wall to Bed Heat Transfer Coefficient," *AIChE J.*, **31**, 127 (1985).

Werther, J., and O. Molerus, "The Local Structure of Gas Fluidized Beds. II: The Spatial Distribution of Bubbles," *Int. J. Multiphase Flow*, **1**, 123 (1973).

Appendix

Integrations used in the derivation of stresses, granular temperature flux, and collisional energy dissipation are given below.

With the Maxwellian distribution given in Eq. 13 and $dc = dC$, we have

$$\tau_{ij}^k = -\epsilon_s\rho_p\langle C_i C_j\rangle = -\epsilon_s\rho_p \frac{1}{n}\int_{-\infty}^{\infty}\frac{n}{(2\pi T)^{3/2}}\exp\left(-\frac{C^2}{2T}\right)C_iC_j dC \quad (A1)$$

$$q_j^k = \epsilon_s\rho_p\left\langle\frac{1}{2}C_iC^2\right\rangle = \frac{1}{2}\epsilon_s\rho_p\frac{1}{n}\int_{-\infty}^{\infty}\frac{n}{(2\pi T)^{3/2}}\exp\left(-\frac{C^2}{2T}\right)C_iC^2 dC \quad (A2)$$

From the definite integrals

$$\int_{-\infty}^{\infty} x^{2n}e^{-\lambda x^2}dx = \frac{(2n-1)!}{2^n}\sqrt{\frac{\pi}{\lambda 2n+1}} \quad (A3)$$

$$\int_{-\infty}^{\infty} x^{2n+1}e^{-\lambda x^2}dx = 0 \quad (A4)$$

we obtain

$$\tau_{ij}^k = -\epsilon_s\rho_p T\delta_{ij} \quad (A5)$$

$$q_j^k = 0 \quad (A6)$$

From Eq. 18, we found that

$$c'_{1j} - c_{1j} = -\tfrac{1}{2}(1+e)(\mathbf{c}_{12}\cdot\mathbf{k})k_j \quad (A7)$$

$$(C_1'^2 - C_1^2) = \tfrac{1}{2}(1+e)(\mathbf{c}_{12}\cdot\mathbf{k})[\tfrac{1}{2}(1+e)(\mathbf{c}_{12}\cdot\mathbf{k}) - 2\,\mathbf{C}_1\cdot\mathbf{k}] \quad (A8)$$

$$(C_2'^2 + C_1'^2 - C_2^2 - C_1^2) = -\tfrac{1}{2}(1-e^2)(\mathbf{c}_{12}\cdot\mathbf{k})^2 \quad (A9)$$

Then, with the definitions of Θ and χ given in Eq. 8, we have

$$\tau_{ij}^c = \Theta_i(mc_j) = \frac{d_p}{2}\int_{\mathbf{c}_{12}\cdot\mathbf{k}>0} -\frac{1}{2}m(1+e)(\mathbf{c}_{12}\cdot\mathbf{k})k_ik_jd_p^2g_0 \cdot\left[f_1f_2 + \frac{1}{2}d_pf_1f_2k_1\frac{\partial}{\partial x_1}\left(\ln\frac{f_1}{f_2}\right)\right]d\mathbf{k}\,d\mathbf{c}_1d\mathbf{c}_2 \quad (A10)$$

$$q_j^c = -\Theta_j\left(\frac{1}{2}mC^2\right) = \frac{d_p}{2}\int_{\mathbf{c}_{12}\cdot\mathbf{k}>0} -\frac{1}{2}m \cdot\left\{\frac{1}{2}(1+e)(\mathbf{c}_{12}\cdot\mathbf{k})\left[\left(\frac{1}{2}(1+e)(\mathbf{c}_{12}\cdot\mathbf{k}) - 2\mathbf{C}_1\cdot\mathbf{k}\right]\right\} \cdot k_jd_p^2g_0\left[f_1f_2 + \frac{1}{2}d_pf_1f_2k_1\frac{\partial}{\partial x_1}\left(\ln\frac{f_1}{f_2}\right)\right]d\mathbf{k}\,d\mathbf{c}_1d\mathbf{c}_2 \quad (A11)$$

$$\gamma = -\chi\left(\frac{1}{2}mC^2\right) = \frac{1}{2}\int_{\mathbf{c}_{12}\cdot\mathbf{k}>0} \cdot\frac{1}{4}m(1-e^2)(\mathbf{c}_{12}\cdot\mathbf{k})^2d_p^2g_0 \cdot\left[f_1f_2 + \frac{1}{2}d_pf_1f_2k_1\frac{\partial}{\partial x_1}\left(\ln\frac{f_1}{f_2}\right)\right]d\mathbf{k}\,d\mathbf{c}_1d\mathbf{c}_2 \quad (A12)$$

were f_1 and f_2 are the Maxwellian distributions at the point $\mathbf{r}$ for particle 1 and particle 2, respectively.

The integrations related to $\mathbf{k}$ are from Chapman and Cowling (1970). Let $\mathbf{h}$, $\mathbf{i}$, and $\mathbf{j}$ denote three mutually perpendicular unit vectors, with $\mathbf{h}$ being in the direction of $\mathbf{c}_{12}$. Let θ and ϕ be the polar angles of $\mathbf{k}$ with respect to $\mathbf{h}$ as axis and the plane of $\mathbf{h}$ and $\mathbf{i}$ as initial plane. Then

$$\mathbf{k} = \mathbf{h}\cos\theta + \mathbf{i}\sin\theta\cos\phi + \mathbf{j}\sin\theta\sin\phi \quad (A13)$$

and

$$d\mathbf{k} = \sin\theta\,d\theta\,d\phi \quad (A14)$$

For a collision occurrence, $\mathbf{c}_{12}\cdot\mathbf{k}$ should be positive. Thus the limits of the integration for $d\theta d\phi$ are: 0 to $\pi/2$ for θ, and 0 to 2π for ϕ. All terms of the integrand containing odd powers of $\sin\phi$

or $\cos\phi$ are zero. Hence,

$$\int (\mathbf{c}_{12} \cdot \mathbf{k})^n \, d\mathbf{k} = \frac{2\pi}{(n+1)} c_{12}^n \tag{A15a}$$

$$\int (\mathbf{c}_{12} \cdot \mathbf{k})^n \, k_i \, d\mathbf{k} = \frac{2\pi}{(n+2)} c_{12}^{n-1} c_{12i} \tag{A15b}$$

$$\int (\mathbf{c}_{12} \cdot \mathbf{k})^n \, k_i \, k_j \, d\mathbf{k} = \frac{2\pi}{(n+1)\,(n+3)} \cdot (n c_{12}^{n-2} c_{12i} c_{12j} + c_{12}^n \delta_{ij}) \tag{A15c}$$

$$\int (\mathbf{c}_{12} \cdot \mathbf{k})^n \, k_i \, k_j \, k_l \, d\mathbf{k} = \frac{2\pi}{(n+2)(n+4)} \cdot [(n-1)\, c_{12}^{n-3} \, c_{12i} c_{12j} c_{12l} + c_{12}^{n-1} (c_{12i} \delta_{jl} + c_{12j} \delta_{il} + c_{12l} \delta_{ij})] \tag{A15d}$$

To obtain the integrations in Eqs. A10–A12, we need to transform the integral variables $d\mathbf{C}_1 \, d\mathbf{C}_2$ to $d\mathbf{C}_{12} d\mathbf{C}_{12}^+$ where

$$\mathbf{C}_1 = \tfrac{1}{2}(\mathbf{C}_{12}^+ + \mathbf{C}_{12}) \tag{A16}$$

and

$$\mathbf{C}_2 = \tfrac{1}{2}(\mathbf{C}_{12}^+ - \mathbf{C}_{12}) \tag{A17}$$

Then we have

$$d\mathbf{c}_1 d\mathbf{c}_2 = d\mathbf{C}_1 d\mathbf{C}_2 = |J| \, d\mathbf{C}_{12} d\mathbf{C}_{12}^+ \tag{A18}$$

with the Jacobian determinant $|J| = 1/8$.

With the above equations, we obtain

$$\tau_{ij}^c = -2\epsilon_s^2 \rho_p g_0 (1+e)\, T \delta_{ij} + \frac{4\epsilon_s^2 \rho_p d_p g_0 (1+e)}{3\pi^{1/2}} T^{1/2} \left(\frac{6}{5} S_{ij} + \frac{\partial v_k}{\partial x_k} \delta_{ij} \right) \tag{A19}$$

$$q_j^c = -2\epsilon_s^2 \rho_p d_p g_0 (1+e) \left(\frac{T}{\pi} \right)^{1/2} \frac{\partial T}{\partial x_j} \tag{A20}$$

$$\gamma = 3(1-e^2)\epsilon_s^2 \rho_p g_0 T \left[\frac{4}{d_p} \left(\frac{T}{\pi} \right)^{1/2} - \frac{\partial v_k}{\partial x_k} \right] \tag{A21}$$

Manuscript received Aug. 31, 1989, and revision received Jan. 4, 1990.